Precise targeting for 3D cryo-correlative light and electron microscopy volume imaging of tissues using a FinderTOP

Marit de Beer[$1,2], Deniz Daviran[$1,2], Rona Roverts[$1,2], Luco Rutten[2], Elena Macías Sánchez[2], Jurriaan R. Metz[3], Nico Sommerdijk[1,2*] , Anat Akiva[1,2*]

[1] Electron Microscopy Center, Radboud Technology Center Microscopy, Radboud University Medical Center, Nijmegen

[2] Department of Biochemistry, Radboud Institute for Molecular Life Sciences, Radboud University Medical Center, Nijmegen

[3] Department of Animal Ecology and Physiology, Radboud Institute for Biological and Environmental Sciences, Faculty of Science, Radboud University, Nijmegen, The Netherlands

$ equal contributions

* Corresponding authors: nico.sommerdijk@radboudumc.nl; anat.akiva@radboudumc.nl

Abstract

Cryo-correlative light and electron microscopy (cryoCLEM) has evolved as a powerful strategy to high resolution imaging in the unperturbed hydrated state, and is now the number one technique for the 3D structural analysis of proteins in their cellular context using cryo-electron tomography (cryoET). In this approach fluorescence microscopy aids in localizing the area of interest, and cryogenic focused ion beam / scanning electron microscopy (cryoFIB/SEM) is used to prepare thin lamellae for cryoET.

While cryoCLEM is now routinely applied to thin on grid lamellae extracted from plunge frozen 2D cell cultures, it cannot address questions related to more complex systems such as tissues and organoids. Here, 3D cryo correlative imaging of large volumes can close the resolution gap between cryo-light microscopy and cryoET, placing the sub-nanometer observations in a larger biological context. Until now, a few technological hurdles made 3D cryoCLEM a challenging, and unexplored approach.

Here we demonstrate a deformation free cryoCLEM workflow for tissues, where we correlate 3D cryo-Airyscan confocal microscopy (cryoCACM) with 3D cryoFIB/SEM volume imaging. Accurate correlation is achieved by imprinting a FinderTOP pattern in the sample surface during high pressure freezing, and allows precise targeting of regions for cryoFIB/SEM volume imaging and cryo-lift out of lamella for cryoTEM.

Introduction

Three dimensional (3D) high resolution imaging is crucial for understanding the structural organization and functioning of cells and tissues[1,2]. For 2D cell cultures, cryo-electron tomography (cryoET) has become available to resolve the structure of proteins within their native cellular context [3,4]. In this context there is an increasing research focus on cryo-correlative light and electron microscopy (cryoCLEM), where fluorescence microscopy aids in localizing the area of interest for high resolution imaging within the cell[5-7], and cryogenic focused ion beam / scanning electron microscopy (cryoFIB/SEM) is used to prepare thin lamellae for cryoEM or cryoET investigation.[8]

Currently, this cryo-CLEM approach is almost exclusively used for the investigation of 2D cell cultures, that are plunge-frozen on a TEM grid. Here, the cell topography and added fiducial markers provide clearly recognizable features that allow straightforward correlation between light and electron images during FIB lamella preparation for cryoEM, where the recently introduced in-SEM-chamber light microscopy increases the success rate of the lamella preparation procedure[9]. However, 2D cell culture models do not suffice for addressing more complex questions that involve cell-cell or cell-matrix interaction, and 3D biological model systems are required[10-13]. The increasing demand for such 3D model systems, including organoids, also demands a different approach to imaging and sample handling.

Plunge freezing cannot be used for tissues due to the limited safe freezing depth (< 5μm), but samples up to 200 μm in thickness can be vitrified in their native state by high pressure freezing (HPF)[14,15]. However, in contrast to cryoCLEM on plunge frozen 2D cell cultures,[16,17] the featureless ice surface of HPF tissue samples prohibits the precise correlation of light and electron images prior to FIB/SEM volume imaging. This is exemplified in the recent demonstration of cryoCLEM for cryo-lift out and cryoET for nematode tissue, where the 2D correlation between light and electron images was limited by the absence of recognizable features.[18]

Nevertheless, a holistic investigation of tissues requires the 3D correlation and analysis of volumes with dimensions that significantly exceed those which can be investigated with cryoET (< 200 nm). This can be achieved through cryoFIB/SEM volume imaging, that allows the detailed nanoscale investigation of vitrified samples with multi-micron dimensions.[19] Nevertheless, to date volume imaging of tissues has mainly been performed using room temperature FIB/SEM[20,21] while only few examples exist of the use 3D cryoFIB/SEM[11,19,22-27] and cryoCLEM volume imaging of tissues is still unchartered territory.

CryoFIB/SEM uses unstained, vitrified samples, while room temperature CLEM volume imaging of tissues so far uses heavy metal staining of plastic embedded samples.[28] Although this produces volume stacks that outclass the raw cryoFIB/SEM data in in signal to noise ratios, the use of stained, dehydrated, embedded samples also has significant drawbacks for CLEM. One is the fluorescence quenching by the staining agents, which necessitates the use of an additional imaging modality (e.g. X-ray computational tomography) for localization of the area of interest. Another one is the need to use microtomy to prepare a starting plane for the FIB milling. A third one is the distortion of the volume due to anisotropic shrinkage of the embedding medium, which impacts the morphological fidelity of 3D images[28].

Here we demonstrate a targeted, distortion free cryoCLEM workflow for tissues, in which 3D cryogenic fluorescence imaging of millimeter scale volumes is precisely correlated to high resolution electron imaging directed by a patterned surface generated during high pressure freezing. We apply this workflow for correlative imaging at the tissue level studying the mineralization process in scales of zebrafish. As a model system for 3D organized organs. In these scales elasmoblasts[29], who's

proteomic profile is near-analogous to human osteoblasts (bone forming cells) produce the extracellular matrix (ECM) that is only partially mineralized to maintain the balance between rigidity and flexibility for both protection and movement[29]. As the elasmoblasts remain active and vital for periods of hours after being removed from the skin the scales form an interesting model to study bone formation processes [30,31].

By uncompromised imaging of tissues in their near-native state over all relevant length scales, from the millimeter down to the nanometer level, this workflow opens up new avenues to study structure-function relations of biological materials, in health and disease.

Results

General work flow. As the zebrafish scales have millimeter dimensions with a thickness in the order of tens of micrometers, we use high pressure freezing for the vitrification. Cryo-Airyscan confocal microscopy (CACM)[17] is used to locate the region of interest (ROI) for 3D cryoFIB/SEM imaging as well as to determine the height, width and dept of the target volume In high pressure frozen tissue samples, however, registration of the two imaging modalities is complicated by the featureless surface of the vitrified ice layer[18]. By using a FinderTOP HPF carrier, a square grid pattern recognizable by both light and electron imaging, is imprinted in the ice surface, after which correlation is achieved computationally through rotational and translational alignment of the imaging modalities. As we are working with native tissue, without beads as fiducial markers, the fluorescent features of the cells are used as recognition points for the fine alignment of the images. 3D cryoFIB/SEM volume imaging is followed by image processing including removal of FIB/SEM artifacts (curtaining, charging), image alignment and contrast enhancement, to reveal the structural details of the sample in its near native state. Comparison of the two imaging modalities shows that, in contrast to room temperature CLEM, no deformation of the tissue occurs during the imaging procedure.

Sample preparation. Regenerating scales were harvested from transgenic zebrafish which have GFP expression under the control of SP7 [32]. SP7 signals the production of osterix, a transcription factor that marks osteoblast formation. Additionally, the freshly harvested scales were fluorescently stained to label the Nucleus (Hoechst) and Mitochondria (MitotrackerRed). After staining, the scales were transferred to a HPF carrier (Ø 3 mm, depth 50 μm) which was topped up with a thin (~8 μm) layer of 10% dextran solution.

The carrier was then closed with a FinderTOP, a typical B type HPF carrier that on its flat side has a matrix with letters and numbers engraved. During vitrification, the engraved square 200 x 200 μm grid pattern of 4μm high lines becomes imprinted in the sample surface (Fig. 1). The surface relief of the pattern is not only in visible in the FIB/SEM, but also in reflection mode cryo-light microscopy due to surface scattering. This is essential for navigation the otherwise featureless sample surface in cryoFIB/SEM[18]. A sacrificial layer of the bilayer membrane forming lipid phosphatidyl choline is applied to the FinderTOP surface to prevent the fracture plane created during opening of the carrier from going through the sample causing the concomitant loss of the imprinted pattern.

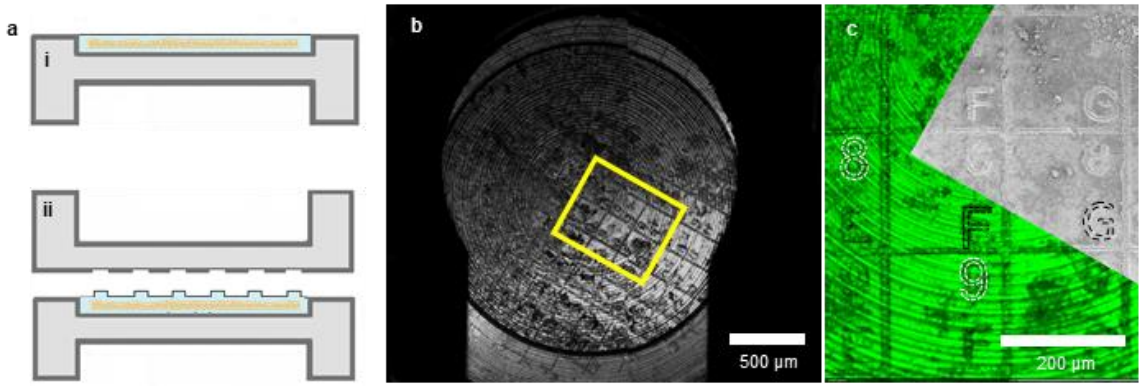

Figure 1. FinderTOP for aligning light and electron images. a) Schematic representation of (i) a HPF carrier representing the featureless surface of tissue sample after vitrification using a conventional flat top carrier compared to (ii) vitrification using the FinderTOP, showing the imprinted pattern on the ice surface. b) Reflection image of the vitrified sample using cryo-light showing the FinderTOP pattern, c) Overlay of the reflection image in the confocal fluorescence microscope (green) with the SEM image in the FIB/SEM (gray).

3D Cryo-fluorescence microcopy. After vitrification, the sample in its 3 mm carrier was loaded into a universal cryo-holder that fixes its position in place, aiding the sample orientation between imaging modalities (Fig. 2). The universal holder was then placed in a cryogenic imaging adaptor and positioned under an upright confocal laser scanning microscope with Airyscan superresolution[5]. To keep registration of the position of the ROI relative to the rest of the sample we build up a series of images with increasing resolution. First, a 2D low resolution overview image (pixel size 624 nm) was recorded of the entire sample for navigation, where the ice surface with FinderTOP pattern was visualized with reflection microscopy (Fig. 2a-i) and the scales with fluorescence microscopy (Fig. 2aii-v). This information was stored in an image correlation program to align and overlay the images and to facilitate further correlation with other imaging modalities.

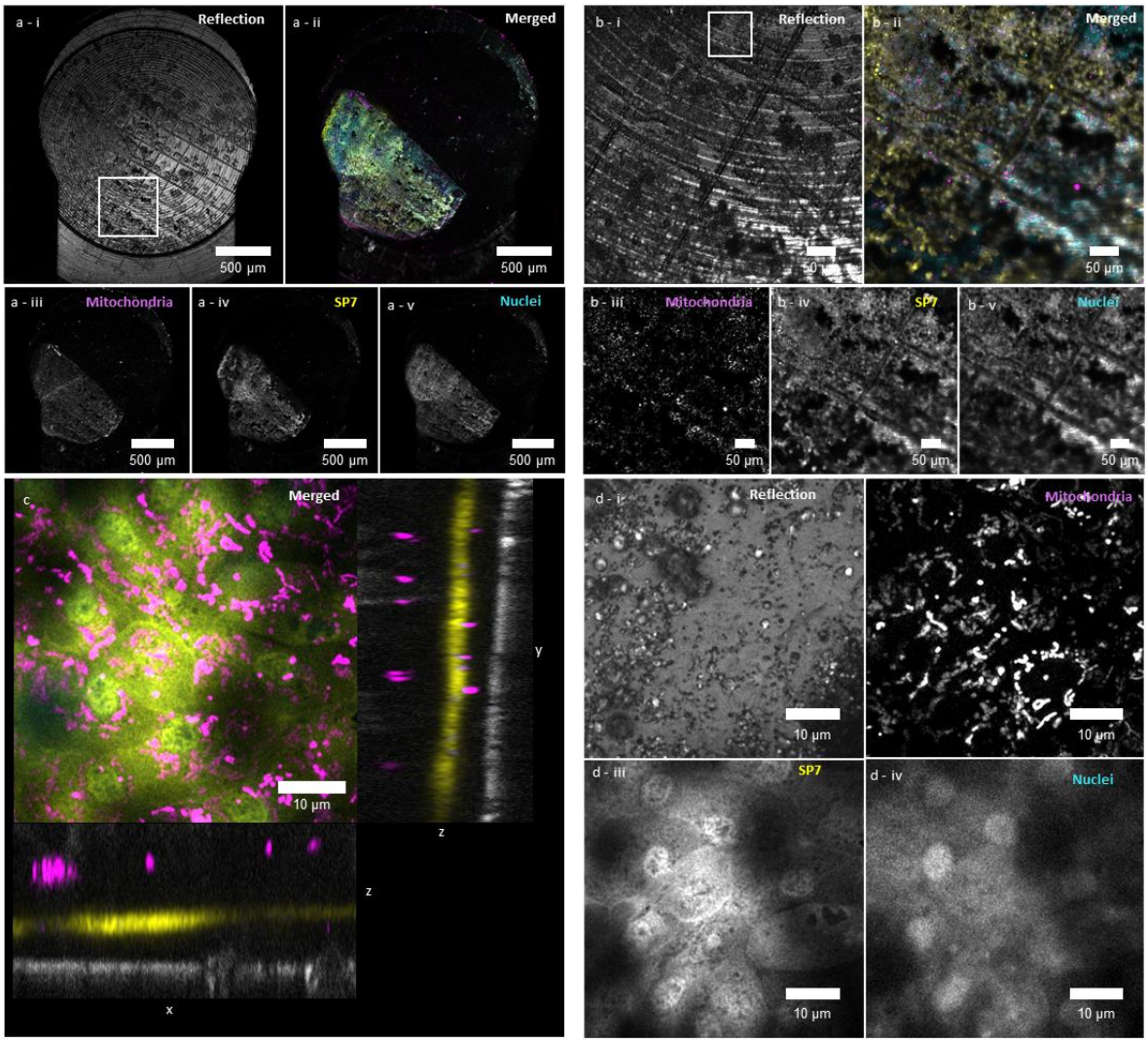

Figure 2. Cryo fluorescence microscopy of the scale. a) Overview images of the scale taken with the 5x objective. a-i) reflection mode shows the FinderTOP imprint. White box indicates the area in b). a-ii) Composite fluorescence image taken with the 10x objective, showing the scale for the different probes in the three channels. a-iii to a-v) Images of the three different fluorescence channels. b) Medium resolution imaging around the region of interest (ROI) using the 10x objective. b-i) Reflection image; the white box denotes the ROI in c). b-ii) Composite image (z-projection of 8 slices) showing the three fluorescent probes and the FinderTop imprint. b-iii to b-v) z-Projection images (8 slices)of the individual fluorescence channels c) High resolution, composite image of the ROI (z-projection of 11 slices) taken with the 100x objective. The image shows the active osteoblast layer with the mitochondrial network. The orthoslices show the cross sectional planes (yz and xz), where also the surface is observed (reflection channel - gray) and the mitochondria in the posterior epithelial cell layer are observed. The orthoslices images are used to calculate the absolute depth of the ROI. d-i to d-iv) z- Projection images (11 slices) of the reflection mode and each fluorescent channel.

As signal-to-noise ratios were low due to the reflection of the ice surface, an additional 3D imaging step (pixel size x-y: 123nm, z: 3000 nm) was used to locate the ROI in 3D (Fig. 2b). This ROI shows an active elasmoblast (fish scale osteoblast) on top of the mineralizing matrix. After overlaying the images in the correlation software, a 3D high resolution (pixel size x-y: 66, z: 360 nm) image of the ROI was recorded for navigation in 3D FIB/SEM volume imaging (Fig 2c). As the tissues sample is covered with a layer of dextran to fill up the volume of carrier above the scale, also high resolution 3D reflection images were recorded to determine the distance of the ROI with respect to the carrier sample surface (Fig 2d). Here, we note that due to optical aberrations introduced by the air-ice interface, the z-distance observed in the cryo-fluorescence images (5,4 µm) deviated by a factor of 1.3 from the actual depth (7.0 µm), as observed in cryoFIB/SEM (See below).

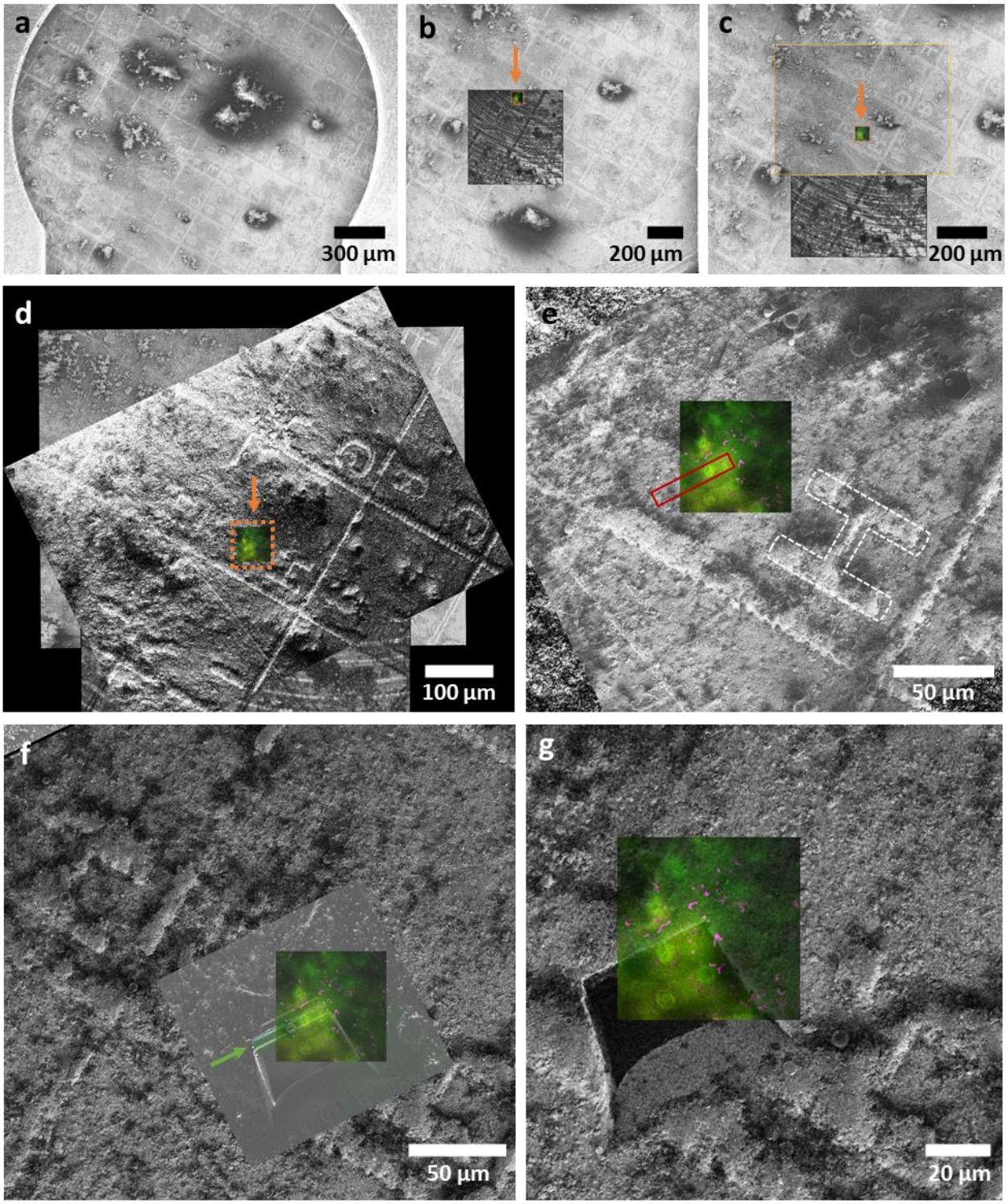

Figure 3. Localization of the region of interest (ROI) in cryoFIB/SEM. a) Low magnification SEM image of the sample, showing the FinderTOP imprint. b) Alignment of the SEM image with the reflection image and the ROI in high resolution CACM (orange box and arrow) using the FinderTOP pattern. c) Higher magnification SEM image (yellow box) overlayed with the images in b), to increase the overlay accuracy. d) SEM images overlayed with FIB image of the ROI, taken in the coincident point and after tilting the sample to 54° (FIB beam perpendicular to the surface). e) Overlay of high magnification FIB image with high resolution CACM image of the ROI and marking of the targeted region for volume imaging (red). f) Overlay of the ROI in CACM and FIB image with showing the milling trench with the SmartFIB view showing the volume stack job (green rectangle, green arrow) in the location of ROI g) FIB image of the trench after milling and recording the image stack.

3D cryoFIB/SEM volume imaging. After transfer to the FIB/SEM, overview secondary electron (SE) images at different magnifications were recorded to align the cryo-SEM view of the FinderTOP surface imprint with the optical overview reflection image of the ice surface and the high resolution CACM image of the ROI within the correlation software (Fig. 3a-c). For fine alignment, a FIB image taken at the coincidence point (with the SEM) was overlayed with already aligned SEM and optical images; (Fig 3d). This enables stage registration and allows using the fluorescence micrographs to navigate to the ROI within the FIB/SEM.

The regions for milling and volume imaging were selected based on the high resolution cryo-fluorescence image and were marked in the correlation software (Fig 3e). For 3D cryoFIB/SEM volume imaging a trench for SEM observation was milled using a high FIB probe current (30 kV@30 nA), where the target depth (30 μm) was determined from the high resolution 3D refection images. The resulting cross section was then polished with a low energy probe (30kV@3nA) to create the first surface for serial surface imaging (Fig. 3f). Subsequently a stack of 97 images was created by alternatingly recording secondary electron (SE) images (pixel size 18 nm) and FIB milling (layer thickness 30 nm), generating a 3D image of 36 x 27 x 2.8 μm (Fig. 3g). During imaging the in-lens secondary electron images were collected at low (2.30 kV) acceleration potential and low (50pA) probe current to avoid beam damage.

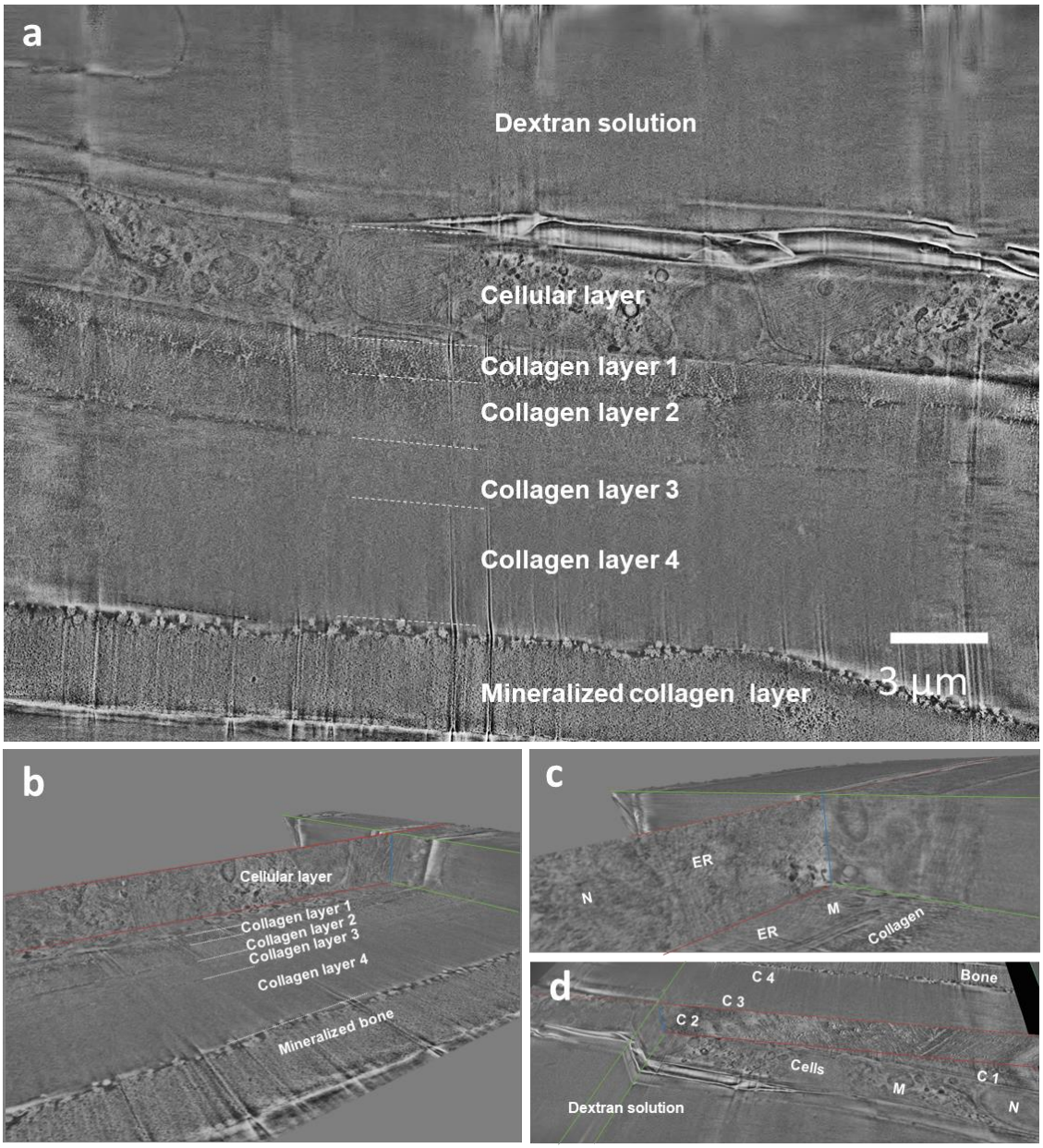

Figure 4. CryoFIB/SEM volume imaging. a) Single secondary electron (SE) image (inLens detector) showing the layered structure of the zebrafish scale. The cellular layer forms the top layer of the tissue and borders with the vitrified dextran solution. Below the cellular layer, there are four distinct collagen layers before reaching the bone-like layer. b) Volume rendering of the cryoFIB/SEM stack showing cross-section of different planes. The different layers of the zebrafish scale tissue are also visible in 3D (see annotations). c-d) Zoom in of the volume image showing c) Details of the cellular layer and d) of the cell-collagen interface. N- Nucleus; M-Mitochondria; ER - Endoplasmatic reticulum; c1-c4 – four collagen layers as described in a) and b).

Image processing

Raw cryoFIB/SEM image stacks suffer from several features that prohibit their direct interpretation and hence their correlation with other imaging modalities (Fig. S1). Firstly, the electron images are recorded from flat featureless surfaces where contrast relies on the variation in electron-sample interaction related to local differences in composition.[19] Next to the fact that these differences are small in biological materials, the low signal-to-noise ratio related to the low applied electron dose further limits the interpretability of the images. Secondly, the image acquisition process itself produces several artifacts, such as inhomogeneous FIB milling (vertical narrow striping: “curtaining”), local

accumulation of electrons in non-conducting surfaces (horizontal broad striping: “charging”) and the skewed brightness across the images due to detector imperfections (uneven illumination).

Using the correlation software package (for details, see materials and methods), first the curtaining was removed after which the local charge imbalance and uneven illumination were simultaneously corrected. This then allowed efficient alignment of the stack that was subsequently denoised after which a final local contrast enhancement step was applied. The processed FIB/SEM images (Fig 4a) now presented a clear cross-sectional view of the scale according to its previously described layered build up[29], revealing the layer of active elasmoblasts on top of layers of collagen with different orientation and structure and below that a layer of bone-like mineralized collagen. 3D visualization afforded the details of the cell layers, including the arrangement of the different organelles with respect to the collagen – cell interface and the particulate structure of the mineralization front (Fig. 4b-d).

Correlation between light and electron imaging. Since the imaging resolution in fluorescence is the limiting factor, the alignment of the two imaging modalities is performed in x-y (imaging) plane of the CACM. For the correlation of the imaging modalities the FIB/SEM data set was re-sliced, and individual corresponding 2D fluorescence - electron image pairs were corrected for the difference in the pixel size between the two imaging modalities. In a set of corresponding images, mitochondria and nuclei were selected as recognizable features and registered visually following a rigid transformation approach (translation and rotation) (Fig 5a). Subsequently, taking the difference in slice thickness into account, another corresponding image pair was chosen 1.5 µm deeper into the sample and the same approach was applied to achieve correlation (Fig 5b). The absence of the need to apply anisotropic scaling or shearing to achieve the same registration as for the first image pair, proves that no deformation (such as shrinkage) occurs during the cryo-workflow, in contrast to what is observed for room temperature CLEM of plastic embedded samples.[28] Registration of the images in both light and electron imaging also demonstrated the accuracy of the correlation during the location of the ROI in the FIB/SEM (Fig 5 c-d).

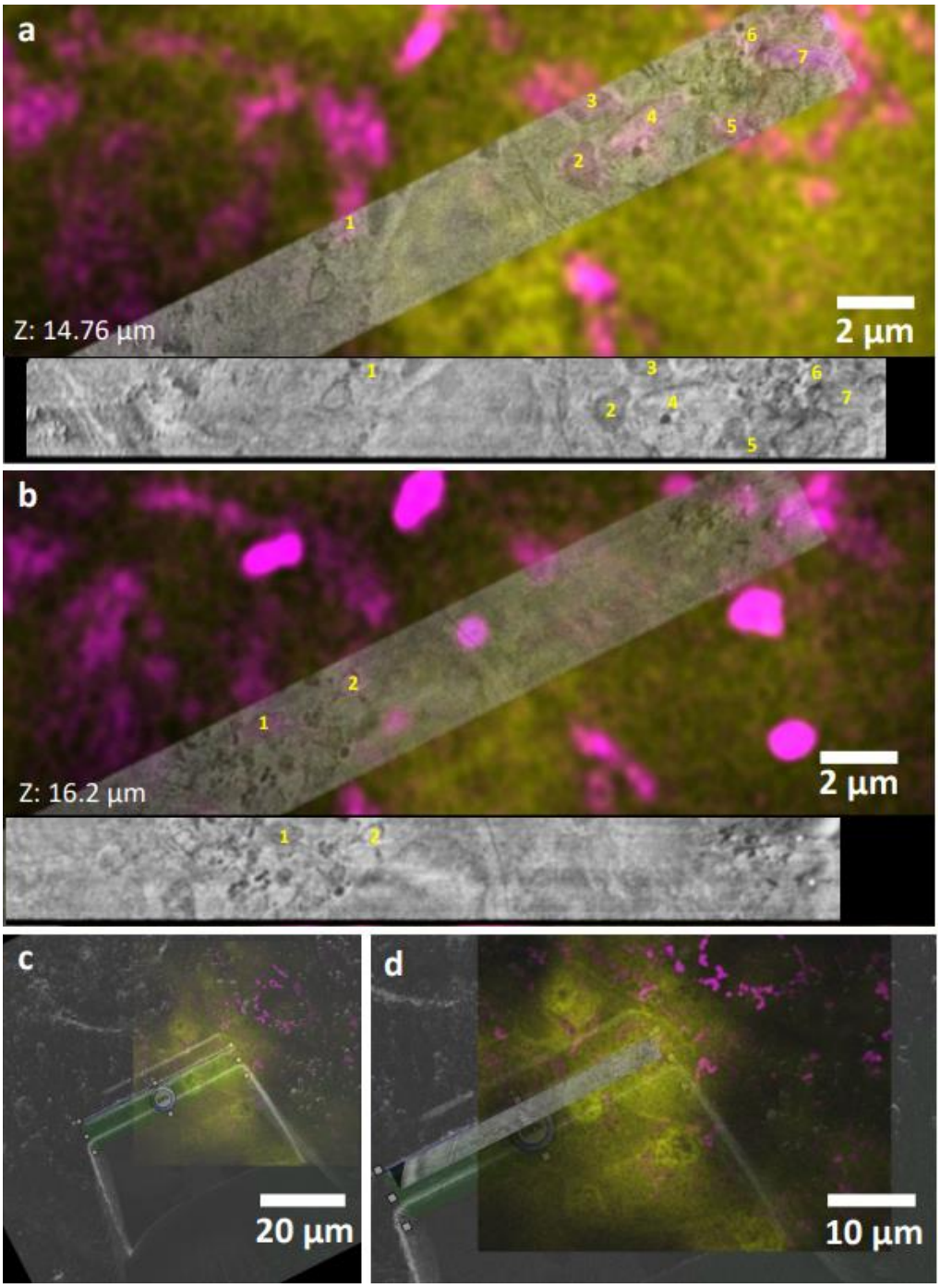

Figure 5. **Alignment of cryoFIB/SEM and CACM images**. a, b) Overlay of single FIB/SEM images from the resliced FIB/SEM stack, manually overlayed and matched with the corresponding the x-y CACM image using the same rigid transformation (translation and rotation). Numbers indicate correlated mitochondria. Insets: corresponding cryoFIB/SEM image. a) z-height 14.76 µm, b) z-height 14.76 µm. c) Superposition of the FIB image and the ROI, showing the milling trench and the selected area for volume imaging. d) Overlay as in c with additional overlay of the recorded and resliced cryoFIB/SEM stack, showing the accuracy of the targeting in cryoCLEM volume imaging.

Cryo-Lift out and cryoTEM. After volume imaging, a lamella for cryoTEM was created by FIB milling (30 kV@30 nA) of a second trench on the backside of the projected lamella, aiming at an initial thickness of ~10 µm (Fig. S2). The precise location and depth of the lamella were determined on the basis of the combined fluorescence and electron volume images. A third, orthogonal trench was prepared to

facilitate the lift out of the lamella with a cryo-gripper as described previously [20]. After lifting out the lamella it was placed on a halfmoon lift-out grid and milled to a thickness of 3 µm with 30kV@3nA probe current, after two windows where thinned to a thickness of less than 200nm for electron transparency in cryoTEM (Fig. S3).

Discussion

Here we demonstrate 3D cryoCLEM volume imaging of 3D tissue samples in their near-native hydrated state, where we are able to select regions based on 3D fluorescence microscopy data to obtain detailed local 3D structural information on cellular and extracellular matrix components, and overlay this with the fluorescence data in 3D. We employ high pressure freezing and cryoFIB/SEM, which allow instantaneous and artifact free cryofixation of large 3D volumes, and high fidelity volume imaging, respectively.

Our approach contrasts the more common cryoCLEM strategy that employs plunge freezing, but which due to the limited safe freezing depth (< 5µm; beyond which crystalline ice is formed that is detrimental for cryoTEM) is restricted to the investigation of 2D cell cultures. Moreover, FIB milling is commonly used for on-grid lamella preparation for cryoEM, but so far there is only one account of 3D FIB/SEM volume imaging of these plunge frozen 2D cell monolayers on TEM grids.[17] Indeed, currently FIB/SEM volume imaging in CLEM has only been used on fixed embedded samples,[20] where anisotropic shrinkage of the plastic embedding matrix leads to deformation of the sample between different imaging modalities.[28] Although cryoFIB/SEM volume imaging is associated with inherent low contrast and acquisition related imaging artefacts, we demonstrate that these limitations can be overcome by applying a designated computational toolbox to remove these artefacts and to enhance contrast

The accuracy of the overlay in cryoCLEM imaging directly depends on the resolution of the optical imaging modality used. In confocal cryo-fluorescence microscopy, resolution is limited by the numerical aperture of the objectives compatible with cryo-imaging[33], with an x-y resolution of 290 nm recently obtained using super resolution CACM of 2D cell cultures[5]. Where correlation with conventional super resolution approaches such as cryo-single molecule localization microscopy provides high resolution fluorescence information and high precision in correlation [34,35], it present limitations with respect to the type and number of dyes that can be used. More precisely, it requires the use of specific photoactivatable dyes, is generally limited to two colors and requires intense laser powers[35,36]. Here we use CACM as it allows the parallel detection of four fluorescence signals, either endogenous labels or infiltrated dyes. In particular the possibility to use the infiltration of dyes is an attractive feature, as it opens up the approach to a wide range of wild type tissues, including human patient materials.

Conclusion

By the incorporation of cryoCACM, high pressure freezing and cryoFIB/SEM in a cryoCLEM workflow, we realized the multiscale imaging of multi cellular systems and tissues in their near-native state, from the millimeter down to the nanometer level - and beyond, through coupling via cryo-lift out to cryoTEM. Accurate correlation is achieved by imprinting a FinderTOP pattern in the sample surface during high pressure freezing, and allows precise targeting of regions for cryoFIB/SEM volume imaging and cryo-lift out of lamella for cryoTEM. Moreover, besides high pressure freezing, this cryo-workflow does not require sample preparation (other than infiltration of fluorescent dyes when wild type tissues are used) and provides correlated high quality 3D FIB/SEM images of cellular and

extracellular details of multi-micron volumes. We expect this correlative cryogenic workflow to open the way to uncompromised targeted high resolution volume imaging of a wide variety of tissues.

Author contributions

N.S and A.A conceived, designed and supervised this study. N.S and A.A acquired funding and administrated the project. M.dB. performed the light microscopy and HPF experiments. D.D performed the image processing and the correlation of light and EM data with support for M.dB. R.R performed the cryoFIB/SEM and lift-out with the aid of M.dB for correlation and localization of ROIs. L.R performed the cryo-TEM experiment with support from E.M.S. J.M. provided the zebrafish scales. N.S and A.A wrote the manuscript with input from all authors.

Acknowledgments

The project was supported by an European Research Council (ERC) Advanced Investigator grant (H2020-ERC-2017-ADV-788982-COLMIN) to N.S. A.A. was also supported by a VENI grant from the Netherlands Scientific Organization NWO (VI.Veni.192.094). E.M.S was supported by a Marie Skłodowska Curie Individual Fellowship (H2020-MSCA-IF-2020- 101031624- DYNAMIN). The authors would like to acknowledge Endre Majorovits and Edwin Lamers from Carl Zeiss for technical support.

Materials and Methods

Zebrafish and scale harvesting

Zebrafish were maintained under normal husbandry conditions as described previously[37]. Transgenic line *Tg(Ola.sp7:NLS-GFP)* were anaesthetized using 0.1% (v/v) 2-phenoxyethanol and placed on a wet tissue containing system water and anesthetic. Scales plucked under a microscope with a watchmaker's tweezers from the midline of the lateral flanks near the dorsal fin.

Fluorescent staining

Fresh harvested scales were fluorescently stained in fish culture medium for at least 2 hours with the following dyes: Mitochondria (100 nM MitoTracker™ Red CMXRos, ThermoFisher, M7512) and Nucleus (1 µg/ml Hoechst 33342, ThermoFisher, H3570). Next, scales were then rinsed in fish culture medium.

High pressure freezing

Scales were immersed in 10% dextran (31349, Sigma) and sandwiched between HPF carriers with 2 mm internal diameter. Prior to creating the sandwich all carriers were rinsed in pure ethanol. The 0.05 mm cavity carrier (Art. 390, Wohlwend) treated with a thin layer of 2% low-melt agarose, to serve as a spacer. A tailor-made grid labeled, flat-sided finderTOP (Alu-platelet labelled, 0.3 mm, Art.1644 Wohlwend) was treated with 1% L-α-phosphatidylcholine (61755, Sigma) in ethanol (1.00983.1000, Supelco). The samples were then high pressure frozen using a HPM Live µ instrument[14] (CryoCapCell) and stored in liquid nitrogen.

The HPF carrier containing the vitrified scales were loaded into a universal cryo-holder (Art. 349559-8100-020, Zeiss cryo accessory kit) using the ZEISS Correlative Cryo Workflow solution, which fit into the PrepDek® (PP3010Z, Quorum technologies, Laughton, UK). This will improve the correlation between cryo-light and cryo-EM.

Fluorescent cryo-imaging

The universal cryo-holder containing the samples was transferred into the Linkam adapter to fit the LSM cryo-stage (CMS-196, Linkam scientific inc.), which was applied to an upright confocal laser

scanning microscopy (LSM 900, Zeiss microscopy GmbH) equipped with an Airyscan 2 detector. First, overview images with low resolution (C Epiplan-Apochromat 5x/0.2 DIC, Zeiss; pixel size 624 nm) were made, to visualize the scales in fluorescence mode (settings described in table 1) and the ice surface in reflection mode. Next, an overlay with the live-cell imaging data was made and 3D images of the ROIs were recorded in medium resolution (C Epiplan-Apochromat 10x/0.4 DIC; pixel size x-y: 123nm, z: 3000 nm). Finally, the ROIs were recorded in 3D with high resolution (C Epiplan-Neofluar 100x/0.75 DIC; pixel size x-y: 66, z: 360 nm) including the reflection microscopy images to measure the dept of the scales within the carrier. Settings had to be adjusted for this 100x objective (Table 2).

Table 2: Cryo-light 100x image acquisition settings

Target	*Excitation*			*Emission*
	Laser (nm)	Laser power (%)	Master gain	*Detection (nm)*
SP7	488	14	900	*490 – 570*
Nucleus Blue	405	25	950	*400 – 490*
Mitotracker	561	17	950	*565 – 620*
Reflection	640	0.2	600	*400 – 700*

CryoFIB/SEM

The correlative cryo holder was mounted in the Quorum shuttle including a cryo lift-out shuttle suited for receiving Omniprobe lift-out grids (Carl Zeiss Microscopy GmbH, Oberkochen, Germany) in the PrepDek® (PP3010Z, Quorum technologies, Laughton, UK). The shuttle was inserted into the Quorum cryo preparation stage with the transfer rod and sputter-coated with platinum, 5mA current for 45 seconds, using the prep stage sputter coater (PP3010T, Quorum technologies, Laughton, UK). After coating, the shuttle was transferred into the Zeiss Crossbeam 550 FIB/SEM (Carl Zeiss Microscopy GmbH, Oberkochen, Germany) using the preparation chamber (PP3010T, Quorum technologies, Laughton, UK). Throughout imaging, the samples were kept at -160 °C and the system vacuum pressure was 2.1 x 10^{-6} mbar.

After inserting the sample into the FIB/SEM chamber, overview SEM images (SE detector) were taken to align the SEM with the LSM reflection image of the ice surface within a single ZEN Connect project. This alignment enables the system registration which allows using the fluorescence signal to navigate to different regions of interest (ROI). To finalize the alignment of the ROI within the FIB/SEM, a FIB image (30kV@10pA probe under 54° tilt) of the surface was collected for a final alignment step with the SEM image.

Course trenches were milled for SEM observation using the 30 kV@30 nA FIB probe. If needed, cold deposition was performed with platinum for 45 sec. The resulting cross section was polished using the 30kV@3nA probe. For volume cryoFIB/SEM imaging of the sample, a stack of 97 images was created by alternatingly recording electron images (both SE and BSE; pixel size 18 nm) and FIB milling (layer thickness 30 nm, FIB probe 30kV@3nA), generating a 3D image of 36 x 27 x 2.8 µm. During imaging in-lens secondary electron imaging and back scatter electron images were simultaneously collected at low (2.30 kV) acceleration potential and low (50pA) probe current to avoid beam damage. The EsB grid was set to 815 V. The image size was set to 2048 × 1536 pixels. For noise reduction line average with a line average count N = 100 at scan speed 1 was used. The voxel size of the stack was 18x18x30 nm. Images were saved in 16 bit .tiff format.

Lift out and cryoTEM.

After volume imaging, a lamella for cryoTEM was created by FIB milling (30 kV@30 nA) of a second trench on the backside of the projected lamella, aiming at an initial thickness of ~10 µm. The precise

location and depth of the lamella were determined on the basis of the combined fluorescence and electron volume images. A third, orthogonal trench was prepared to facilitate the lift-out of the lamella with a cryo-gripper as described previously[20]. After lifting out the lamella it was placed on a halfmoon lift-out grid (Omniprobe). Milling into the copper grid causes redeposition to 'glue' the lamella onto the grid. To protect the lamella, its top surface was covered with a cold deposition platinum layer. The complete lamella was thinned to a thickness of ~3 µm with 30kV;3nA probe current. 2 windows where thinned to a thickness of less than 200nm for electron transparency with small steps using subsequently the following probe currents: 30kV@700pAa, 30kV@300pA, 30kV@100pA. Final polishing was performed with 30kV;50pA probe current. A JEOL JEM-2100 system (JEOL Ltd., Tokyo, Japan) equipped with Gatan 914 high tilt cryo holder and a LaB6 filament was used for cryogenic imaging at 200 kV. Images were recorded with a Gatan 890 Ultrascan (Pleasanton, CA, USA) using low dose software (Serial EM, total dose < 20 e-/$Å^2$).

Image Processing

The cryoFIB/SEM images were processed using the EM processing toolbox of Zen Connect 3.5 (blue edition) to correct for defects such as curtaining, misalignment and local charging, analogous to our previously reported approach[38], but with keeping the same processing settings for the whole stack. The same software was used for subsequent noise reduction and contrast enhancement. A summary of each processing step is as follows:

Curtaining: Removing the vertical stripes in the stacks was done using the "variational stationary noise removal" approach with only one filter in which the maximum level of noise allowed by the software was selected.

Charging: Elimination of the local charge imbalance and uneven illumination was achieved by using anisotropic gaussian background subtraction. Briefly, a mask with maximum sigma in the x direction and minimum sigma in the y direction was created using the "Gauss" option in the toolbox. Subsequently, this mask was subtracted from the destriped image to obtain the charge balanced image. This approach simultaneously corrects any potential uneven illumination as well.

Alignment: To make sure that all the misalignments in the stack are in the same range, a manual alignment was initially done using the "Coarse Z-stack alignment" option in the toolbox. Subsequently, the smaller misalignments were corrected using "Z-stack alignment with ROI" option in the toolbox in which we only allowed for translational registration.

Noise Reduction: In order to improve the signal-to-noise ratio, noise reduction was performed using the "Denoise" option in the toolbox. The chosen denoising method was "Real wavelets" with a moderate strength.

Contrast enhancement: As the final processing step, the contrast was enhanced using "Enhance local contrast" option in the toolbox. To avoid over-amplification of homogeneous regions, we opted for a small clip limit.

Ethics declaration

Ethics approval and consent to participate

Animal research that is presented in this work has been conducted with ethical approval following the ARRIVE guidelines. Experiments were locally ethically reviewed by Radboud University (Nijmegen, NL) and performed under RU-DEC2014-059 (RU).

REFERENCES

1 Nakane, T. *et al.* Single-particle cryo-EM at atomic resolution. *Nature* **587**, 152-156, doi:10.1038/s41586-020-2829-0 (2020).

2 *The Nobel Prize in Chemistry 2017. NobelPrize.org. Nobel Prize Outreach AB 2022. Mon. 18 Jul 2022. <https://www.nobelprize.org/prizes/chemistry/2017/summary/>*.

3 Medalia, O. *et al.* Macromolecular architecture in eukaryotic cells visualized by cryoelectron tomography. *Science* **298**, 1209-1213, doi:10.1126/science.1076184 (2002).

4 Chmielewski, D., Schmid, M. F., Simmons, G., Jin, J. & Chiu, W. Chikungunya virus assembly and budding visualized in situ using cryogenic electron tomography. *Nat Microbiol*, doi:10.1038/s41564-022-01164-2 (2022).

5 Sexton, D. L., Burgold, S., Schertel, A. & Tocheva, E. I. Super-resolution confocal cryo-CLEM with cryo-FIB milling for in situ imaging of Deinococcus radiodurans. *Curr Res Struct Biol* **4**, 1-9, doi:10.1016/j.crstbi.2021.12.001 (2022).

6 Gupta, T. K. *et al.* Structural basis for VIPP1 oligomerization and maintenance of thylakoid membrane integrity. *Cell* **184**, 3643-3659.e3623, doi:10.1016/j.cell.2021.05.011 (2021).

7 Fermie, J. *et al.* Bimodal endocytic probe for three-dimensional correlative light and electron microscopy. *Cell Rep Methods* **2**, 100220, doi:10.1016/j.crmeth.2022.100220 (2022).

8 Mahamid, J. *et al.* Visualizing the molecular sociology at the HeLa cell nuclear periphery. *Science* **351**, 969-972, doi:doi:10.1126/science.aad8857 (2016).

9 Smeets, M. *et al.* Integrated Cryo-Correlative Microscopy for Targeted Structural Investigation In Situ. *Microscopy Today* **29**, 20-25, doi:10.1017/S1551929521001280 (2021).

10 Akiva, A. *et al.* An Organoid for Woven Bone. *Advanced Functional Materials* **31**, 2010524, doi:https://doi.org/10.1002/adfm.202010524 (2021).

11 Akiva, A. *et al.* Intercellular pathways from the vasculature to the forming bone in the zebrafish larval caudal fin: Possible role in bone formation. *Journal of Structural Biology* **206**, 139-148, doi:10.1016/j.jsb.2019.02.011 (2019).

12 Lamers, M. M. *et al.* SARS-CoV-2 productively infects human gut enterocytes. *Science* **369**, 50-54, doi:10.1126/science.abc1669 (2020).

13 Jansen, J. *et al.* SARS-CoV-2 infects the human kidney and drives fibrosis in kidney organoids. *Cell Stem Cell* **29**, 217-231.e218, doi:10.1016/j.stem.2021.12.010 (2022).

14 Heiligenstein, X. *et al.* HPM live mu for a full CLEM workflow. *Methods Cell Biol* **162**, 115-149, doi:10.1016/bs.mcb.2020.10.022 (2021).

15 Shimoni, E. & Müller, M. On optimizing high-pressure freezing: from heat transfer theory to a new microbiopsy device. *J Microsc* **192**, 236-247, doi:10.1046/j.1365-2818.1998.00389.x (1998).

16 Klein, S., Wachsmuth-Melm, M., Winter, S. L., Kolovou, A. & Chlanda, P. in *Methods in Cell Biology* Vol. 162 (eds Thomas Müller-Reichert & Paul Verkade) 273-302 (Academic Press, 2021).

17 Wu, G. H. *et al.* Multi-scale 3D Cryo-Correlative Microscopy for Vitrified Cells. *Structure* **28**, 1231-1237.e1233, doi:10.1016/j.str.2020.07.017 (2020).

18 Schaffer, M. *et al.* A cryo-FIB lift-out technique enables molecular-resolution cryo-ET within native Caenorhabditis elegans tissue. *Nature Methods* **16**, 757-762, doi:10.1038/s41592-019-0497-5 (2019).

19 Vidavsky, N. *et al.* Cryo-FIB-SEM serial milling and block face imaging: Large volume structural analysis of biological tissues preserved close to their native state. *J Struct Biol* **196**, 487-495, doi:10.1016/j.jsb.2016.09.016 (2016).

20 Ronchi, P. *et al.* High-precision targeting workflow for volume electron microscopy. *Journal of Cell Biology* **220**, doi:10.1083/jcb.202104069 (2021).

21 Xu, C. S. *et al.* Enhanced FIB-SEM systems for large-volume 3D imaging. *Elife* **6**, doi:10.7554/eLife.25916 (2017).

22 Schertel, A. *et al.* Cryo FIB-SEM: volume imaging of cellular ultrastructure in native frozen specimens. *J Struct Biol* **184**, 355-360, doi:10.1016/j.jsb.2013.09.024 (2013).
23 Vidavsky, N., Masic, A., Schertel, A., Weiner, S. & Addadi, L. Mineral-bearing vesicle transport in sea urchin embryos. *J Struct Biol* **192**, 358-365, doi:10.1016/j.jsb.2015.09.017 (2015).
24 Varsano, N. *et al.* Characterization of the growth plate-bone interphase region using cryo-FIB SEM 3D volume imaging. *J Struct Biol* **213**, 107781, doi:10.1016/j.jsb.2021.107781 (2021).
25 Friedman, O. *et al.* Structural organization of xanthine crystals in the median ocellus of a member of the ancestral insect group Archaeognatha. *J Struct Biol* **214**, 107834, doi:10.1016/j.jsb.2022.107834 (2022).
26 Zhu, Y. *et al.* Serial cryoFIB/SEM Reveals Cytoarchitectural Disruptions in Leigh Syndrome Patient Cells. *Structure* **29**, 82-87.e83, doi:https://doi.org/10.1016/j.str.2020.10.003 (2021).
27 Klumpe, S. *et al.* A modular platform for automated cryo-FIB workflows. *eLife* **10**, e70506, doi:10.7554/eLife.70506 (2021).
28 Hoffman, D. P. *et al.* Correlative three-dimensional super-resolution and block-face electron microscopy of whole vitreously frozen cells. *Science* **367**, doi:10.1126/science.aaz5357 (2020).
29 Sire, J. Y. & Akimenko, M. A. Scale development in fish: a review, with description of sonic hedgehog (shh) expression in the zebrafish (Danio rerio). *Int J Dev Biol* **48**, 233-247, doi:10.1387/ijdb.15272389 (2004).
30 Pasqualetti, S., Banfi, G. & Mariotti, M. The zebrafish scale as model to study the bone mineralization process. *J Mol Histol* **43**, 589-595, doi:10.1007/s10735-012-9425-z (2012).
31 de Vrieze, E., Sharif, F., Metz, J. R., Flik, G. & Richardson, M. K. Matrix metalloproteinases in osteoclasts of ontogenetic and regenerating zebrafish scales. *Bone* **48**, 704-712, doi:10.1016/j.bone.2010.12.017 (2011).
32 DeLaurier, A. *et al.* Zebrafish sp7:EGFP: a transgenic for studying otic vesicle formation, skeletogenesis, and bone regeneration. *Genesis* **48**, 505-511, doi:10.1002/dvg.20639 (2010).
33 Mahamid, J. *et al.* A focused ion beam milling and lift-out approach for site-specific preparation of frozen-hydrated lamellas from multicellular organisms. *J Struct Biol* **192**, 262-269, doi:10.1016/j.jsb.2015.07.012 (2015).
34 Liu, B. *et al.* Three-dimensional super-resolution protein localization correlated with vitrified cellular context. *Sci Rep* **5**, 13017, doi:10.1038/srep13017 (2015).
35 Tuijtel, M. W., Koster, A. J., Jakobs, S., Faas, F. G. A. & Sharp, T. H. Correlative cryo super-resolution light and electron microscopy on mammalian cells using fluorescent proteins. *Sci Rep* **9**, 1369, doi:10.1038/s41598-018-37728-8 (2019).
36 Chang, Y. W. *et al.* Correlated cryogenic photoactivated localization microscopy and cryo-electron tomography. *Nat Methods* **11**, 737-739, doi:10.1038/nmeth.2961 (2014).
37 Bergen, D. J. M. *et al.* Regenerating zebrafish scales express a subset of evolutionary conserved genes involved in human skeletal disease. *BMC Biology* **20**, 21, doi:10.1186/s12915-021-01209-8 (2022).
38 Kapteijn, R. *et al.* DNA uptake by cell wall-deficient bacteria reveals a putative ancient macromolecule uptake mechanism. *bioRxiv*, 2022.2001.2027.478057, doi:10.1101/2022.01.27.478057 (2022).

Supporting information for

Precise targeting for 3D cryo-correlative light and electron microscopy volume imaging of tissues using a FinderTOP

Marit de Beer[$1,2], Deniz Daviran[$1,2], Rona Roverts[$1,2], Luco Rutten[2], Elena Macias[2], Jurriaan Metz[3], **Nico Sommerdijk[1,2*] , Anat Akiva[1,2*]**

[1] Electron Microscopy Center, Radboud Technology Center Microscopy, Radboud University Medical Center, Nijmegen

[2] Department of Biochemistry, Radboud Institute for Molecular Life Sciences, Radboud University Medical Center, Nijmegen

[3] Department of Animal Ecology and Physiology, Radboud Institute for Biological and Environmental Sciences, Faculty of Science, Radboud University, Nijmegen, The Netherlands

$ equal contributions

* Corresponding authors: nico.sommerdijk@radboudumc.nl; anat.akiva@radboudumc.nl

Figure S1. Unprocessed secondary electron image in cryoFIB/SEM

Figure S2. Cryo Lamella lift out

Figure S3. CryoTEM imaging

Figure S1. Unprocessed secondary electron image in cryoFIB/SEM. Raw secondary electron image (InLense detector) in cryoFIB/SEM before processing showing low-signal-to-noise ratios (low contrast) due to the low electron dose used for imaging (avoiding electron beam damage). Image also contains the typical FIB/SEM acquisition artefacts including vertical striping ("curtaining") due to uneven FIB milling, horizontal striping due to charging, and uneven illumination due to inhomogeneous detector sensitivity.

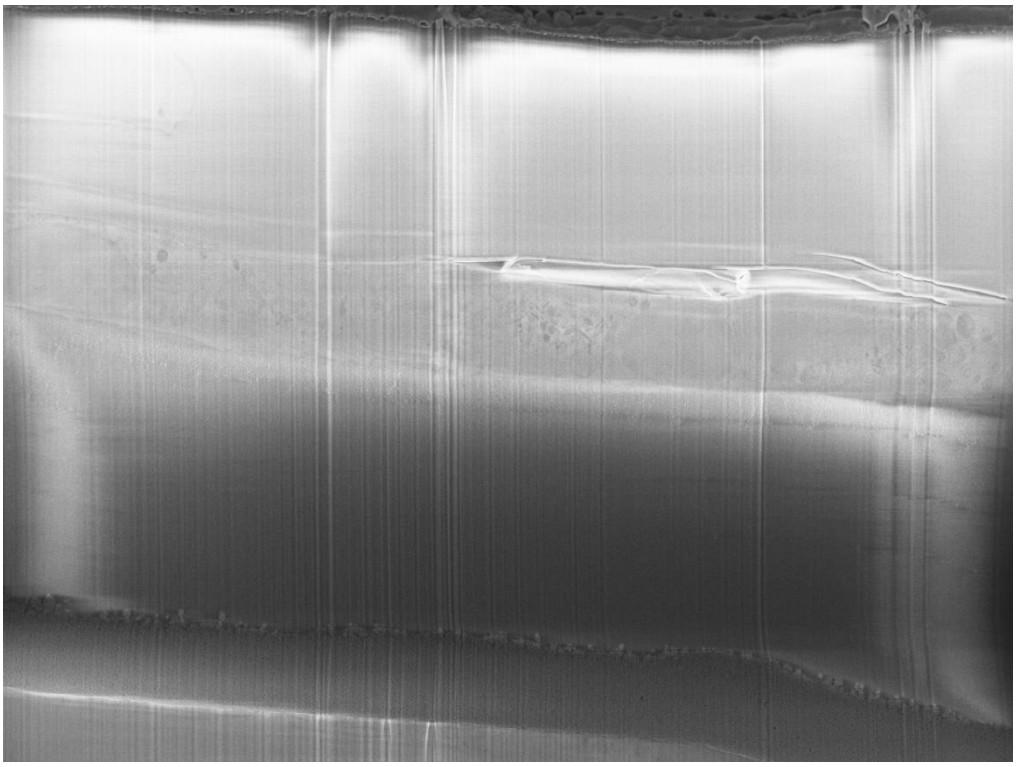

Figure S2. Cryo Lamella lift out. a) Low magnification SEM (SE) overview of the sample with FinderTOP. b) FIB image of the trench after volume imaging, c) FIB image of the lamella after milling the second trench. d) SEM image (BSE) after milling the lift out trench, e) SEM image (SE) of the gripper taking the lamella, f) SEM image (SE) of the gripper positioning the lamella on the halfmoon lift-out grid. g) SEM image (SE) of the lamella mounted on the halfmoon lift out grid. h) zoom in of g) showing the metal deposits connecting lamella and grid. I) FIB image after thinning the lamella showing the 3µm supports (red arrows) between the electron transparent windows (yellow arrows) for cryoTEM.

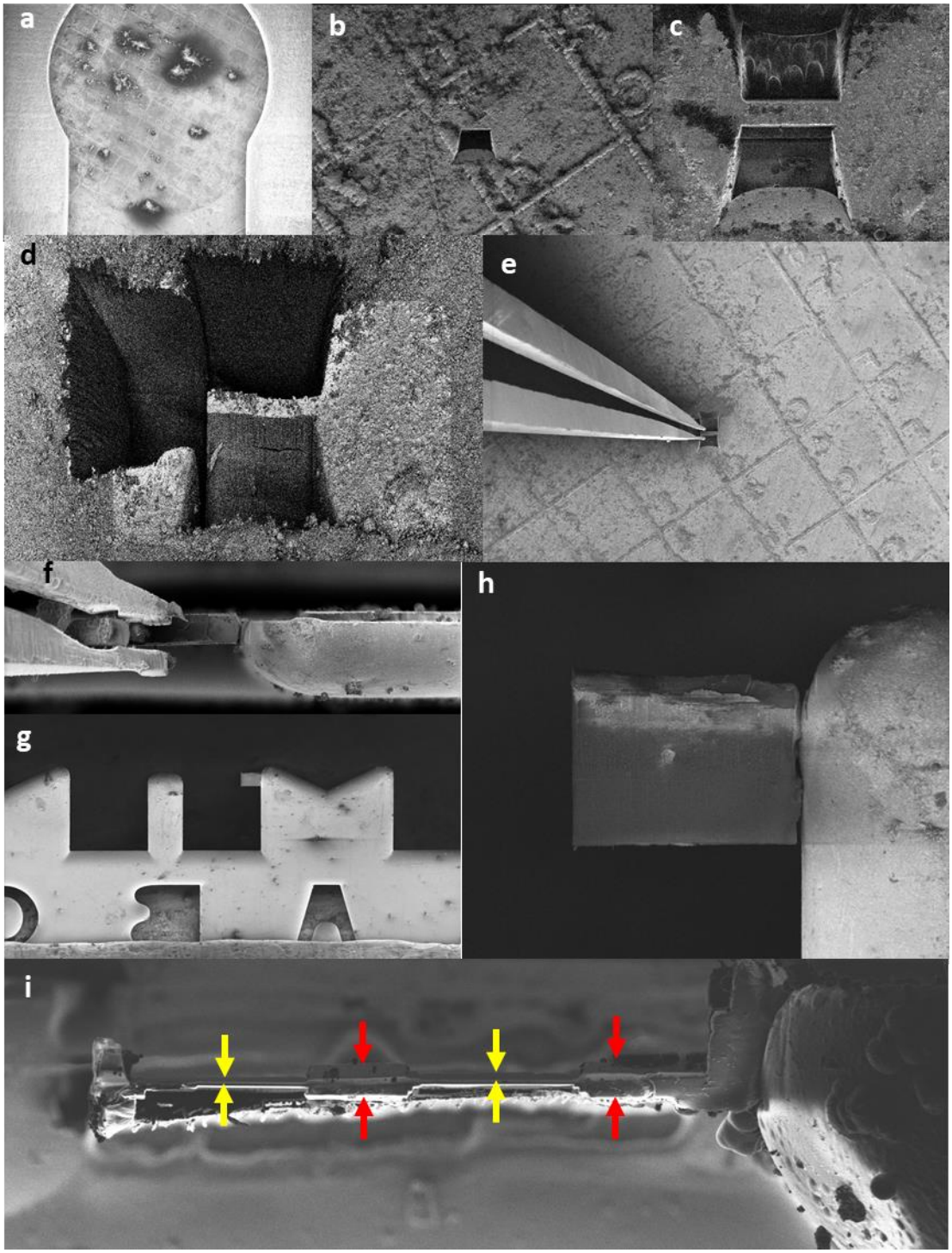
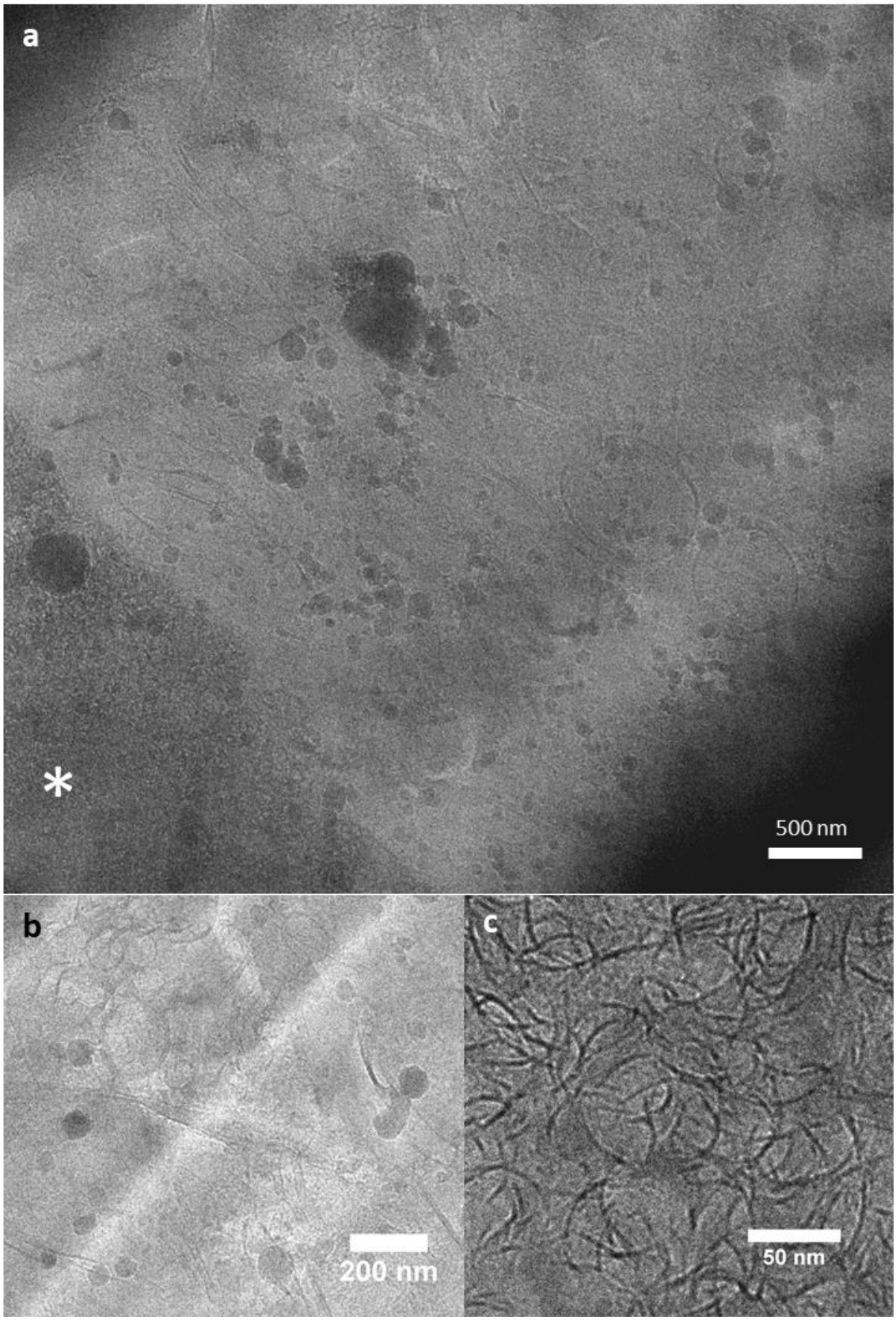
Figure S3. CryoTEM imaging. CryoTEM image of a lift-out lamella showing a) the cell mineral interface on the posterior side of the scale [29]. Mineral layer is marked with asterix (∗). b) zoom-in of the cellular layer, c) zoom in of the mineral layer.